Photoelectrochemical biosensing of disease marker on p-type Cu-doped $Zn_{0.3}Cd_{0.7}S$ based on RCA and exonuclease III amplification

Kangyao Zhang, Shuzhen Lv, Minghua Lu, Dianping Tang

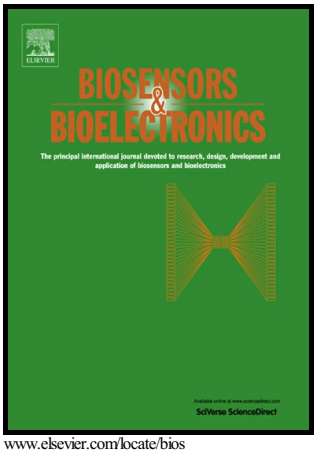

www.elsevier.com/locate/bios

PII: S0956-5663(18)30502-5
DOI: https://doi.org/10.1016/j.bios.2018.07.001
Reference: BIOS10590

To appear in: *Biosensors and Bioelectronic*

Received date: 15 May 2018
Revised date: 9 June 2018
Accepted date: 1 July 2018

Cite this article as: Kangyao Zhang, Shuzhen Lv, Minghua Lu and Dianping Tang, Photoelectrochemical biosensing of disease marker on p-type Cu-doped $Zn_{0.3}Cd_{0.7}S$ based on RCA and exonuclease III amplification, *Biosensors and Bioelectronic,* https://doi.org/10.1016/j.bios.2018.07.001

Photoelectrochemical biosensing of disease marker on p-type Cu-doped $Zn_{0.3}Cd_{0.7}S$ based on RCA and exonuclease III amplification

Kangyao Zhang[a], Shuzhen Lv[a], Minghua Lu[b*], Dianping Tang[a*]

[a]Key Laboratory for Analytical Science of Food Safety and Biology (MOE & Fujian Province), Department of Chemistry, Fuzhou University, Fuzhou 350116, P.R. China

[b]Institute of Environmental and Analytical Science, School of Chemistry and Chemical Engineering, Henan University, Kaifeng 475004, Henan, P.R. China

minghualu88@yeah.net
dianping.tang@fzu.edu.cn

[*]Corresponding authors. Tel,/fax: +86 591 2286 6125.

ABSTRACT

In this work, a new "signal-on" split-type photoelectrochemical (PEC) sensing platform for prostate-specific antibody (PSA) detection was successfully constructed using p-type Cu-doped $Zn_{0.3}Cd_{0.7}S$ as the photosensitive semiconductor material and target-triggered rolling circle amplification (RCA) for signal amplification. The signal derived from Cu-doped $Zn_{0.3}Cd_{0.7}S$ was amplified by hemin/G-quadruplex. Upon target PSA introduction, the aptamer-primer probe (apt-pri) was captured by capture antibody-conjugated magnetic bead (MB-mAb) to form the sandwiched MB-mAb/PSA/apt-pri. The complex could initiate the RCA reaction to produce a long single-stranded DNA that provided binding sites for G-rich DNA and to form long single-stranded DNA/G-quadruplex/hemin. Upon the addition of exonuclease III (Exo III), the hemin/G-quadruplex immobilized on the RCA long product could be released by the digestion of Exo III. The hemin/G-quadruplex complexes in this study were used as efficient electron acceptors to neutralize the photoelectrons generated from the semiconductor and hindered the recombination of charges,

thus enhancing the photocurrent. Under the optimum conditions, the developed sensing system displayed a good analytical performance with a linear range of 0.05 - 40 ng mL^{-1} PSA and a detection limit of 16.3 pg mL^{-1}. Furthermore, good selectivity, high anti-interference ability, satisfactory reproducibility, and good accuracy were also achieved. These prominent analytical properties revealed that our strategy might be a potential and reliable tool for the detection of PSA.

KEYWORDS: photoelectrochemical biosensor; Cu-doped $Zn_{0.3}Cd_{0.7}S$; rolling circle amplification; exonuclease III; hemin/G-quadruplex

1. Introduction

Sensitive and specific monitoring of disease-related proteins is critical to the early diagnosis and screening of diseases such as cancer (Kulasingam et al., 2008). As far as we know, the concentration of biomarkers is at a low level in the early stages of cancer. Thus, it is meaningful to develop simple, fast and effective analytical methods to meet the growing demand for the detection of low-abundance tumor markers in biological fluids (Chinen et al, 2015; Eivazzadeh-Keihan et al., 2018). Recently, photoelectrochemical (PEC) sensing methods have been receiving increasing interest in the bioanalytical community because the technique has the advantages of easy operation, low cost, and easy micromation of the instrument (Cong et al., 2016; Fan et al., 2017). In addition, the PEC assays could provide remarkable sensitivity and low background signal due to the difference in energy form between the input and output (light as the excitation source, and electricity as the readout signal) (Wang et al., 2012; Chen et al., 2017). The role of the photoelectrode in the PEC process is to achieve the conversion of light to electrical signal, therefore, the photoelectrode has a significant impact on the analytical performance of PEC sensors. To date, the most widely used photosensitive materials in PEC sensors belong to n-type semiconductors (*e.g.*, CdS and TiO_2) (Zhang et al., 2018; Zhao et al., 2013) or sensitized n-type semiconductors (*e.g.*, Au/$BiVO_4$, CdSe/TiO_2, and IrO_2/Hemin/TiO_2) (Shu et al., 2016; Pang et al., 2015; Tang et al., 2013). Unfortunately, the practical applications of these n-type semiconductors are easily disturbed by the

coexistence of reductive substances such as ascorbic acid, dopamine, and those compounds in sophisticated biological fluids because of the high oxidation activity of the photogenerated holes at the semiconductor/electrolyte interface (Li et al., 2015; Wang et al., 2015; Lv et al., 2017). As opposed to n-type semiconductors, p-type semiconductors are more likely to interact with oxidize agents (*i.e.*, electron acceptors) rather than with reductive agents (*i.e.*, electron donors) on account of the high reduction activity of the photogenerated electrons, which indicates that they have excellent performance in terms of anti-interference of reductive substances (Dai et al., 2017). Despite their many attractions for PEC analysis, research in this area has lagged far behind. Thus, it is worthwhile to enlarge the application of such p-type semiconductors in the PEC bioanalysis. Recently, Zhu's group has exploited a novel p-type semiconductor for water splitting (Wu et al., 2016a). They found that the traditional n-type $Zn_xCd_{1-x}S$ solid solutions turned into a p-type semiconductor when cuprous ions were employed for doping during the synthesis process. As a typical binary II−VI semiconductor, $Zn_xCd_{1-x}S$ nanocrystals have been widely studied because of their tunable bandgap width properties and prominent electrical conductivity (Li et al., 2011; Xu et al., 2012). As is known to all, when the wide bandgap and the narrow bandgap semiconductor form solid solutions, the bandgap width of the newly formed nanocrystals can be continuously variable (Li et al., 2008). Thus, through altering the compositions (the molar ratio of Zn:Cd), it is possible to synthesize a nanocomposite with an appropriate band gap energy and a suitable band position that can drive redox reaction under light irradiation (Kaur et al., 2017). On the basis of the advantages of $Zn_xCd_{1-x}S$ and Zhu's work, the construction of p-type Cu-doped $Zn_{0.3}Cd_{0.7}S$-based PEC sensing platform for the analytical fields would obviously be desirable.

Hemin/G-quadruplex, which belongs to the DNAzymes, contains the characteristics of DNA sequences (easy synthesis, low cost of production, and thermal stability) and hemin (horseradish peroxidase-mimicking activity) (Deng et al., 2008; Tang et al., 2016), and has been considered as an ideal candidate for exploiting versatile bioanalysis methods. Up to now, various analytical techniques based on the catalytic activity of hemin/G-quadruplex have been reported for the detection of analytes, including colorimetry (Zhou et al., 2013; Ren et al., 2015), electrochemistry (Liu et al., 2017; Alizadeh et al., 2017), and chemiluminescence (Gao et al., 2013; Zhou et al., 2014). Apart from the peroxidase-like activity, it is interesting to note that hemin/G-quadruplex has been shown to possess the ability to act as an electron acceptor. In 2010, Sharon et al. demonstrated

the process of electron transfer between CdSe/ZnS quantum dots and the hemin/G-quadruplex complex for the first time and developed a fluorescence aptasensor based on this novel mechanism (Sharon et al., 2010). To reduce the possibility of false positives of abovementioned strategy, Wang et al. reported a "signal-on" PEC biosensing platform on the basis of the target-induced conformational conversion and photoinduced electron transfer (PET) mechanism (Wang et al., 2015).

Prostate-specific antigen (PSA), which has been known as the most reliable and specific biomarker for the early diagnosis of prostate cancer, is present in the blood serum of healthy males (the normal levels are below 4.0 ng mL^{-1}), and the elevated concentration of PSA could be used to indicate the health state of prostate. By integrating p-type Cu-doped $Zn_{0.3}Cd_{0.7}S$, rolling circle amplification (RCA), and hemin/G-quadruplex, our group herein designed a novel PEC sensing mode for PSA detection (Scheme 1). Specifically, capture antibody coated magnetic bead is utilized to capture the aptamer-primer probe in the presence of PSA. After that, RCA reaction is performed with the assistance of padlock DNA and enzymes (*i.e.*, T4 DNA ligase and Phi29 DNA polymerase). The long single-stranded DNA generated by the RCA reaction ensures the introduction of G-rich DNA and the formation of long single-stranded DNA/G-quadruplex/hemin. Thereafter, hemin/G-quadruplex is released by the digestion of exonuclease III. When p-type Cu-doped $Zn_{0.3}Cd_{0.7}S$ is irradiated under the light, these free hemin/G-quadruplex complexes can accept the photogenerated electrons from semiconductor to significantly enhance the photocurrent response. Thus, the quantitative detection of PSA concentration in the sample can be achieved by monitoring the change of cathodic photocurrent.

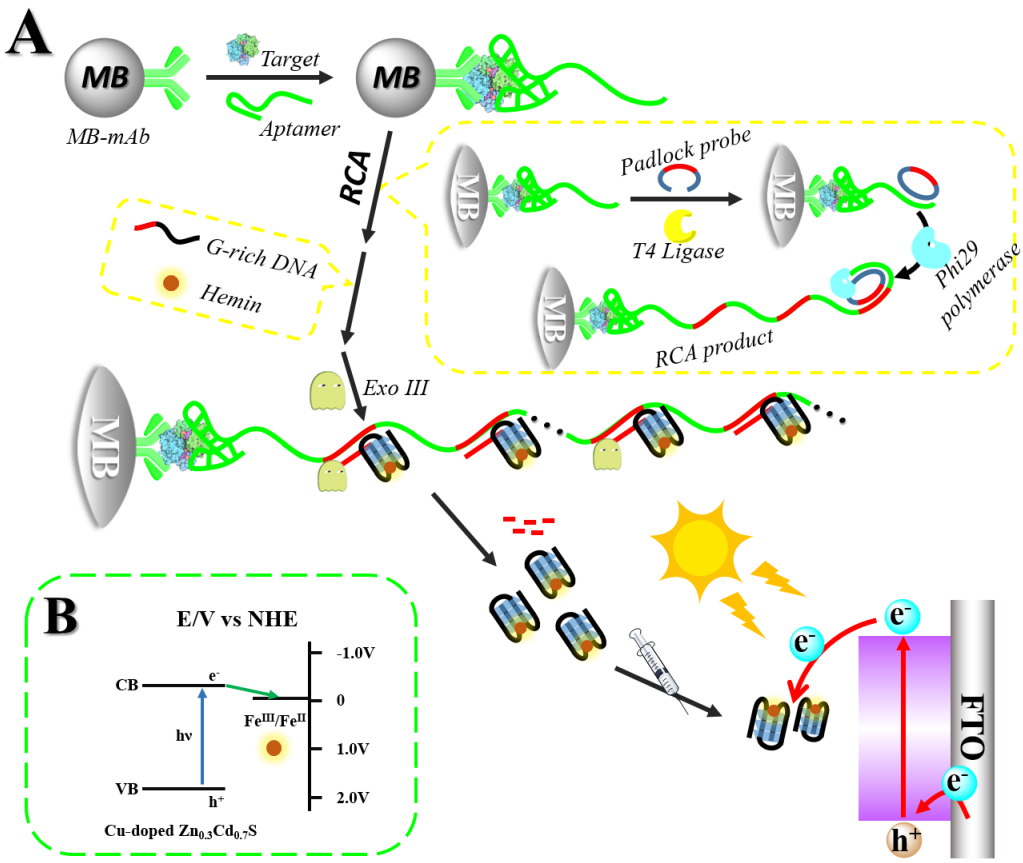

Scheme 1. (A) Schematic illustration of p-type Cu-doped $Zn_{0.3}Cd_{0.7}S$-based photoelectrochemical sensing platform; and (B) the comparison of energy levels diagram of hemin/G-quadruplex complex and p-type Cu-doped $Zn_{0.3}Cd_{0.7}S$.

2. Experimental

2.1. Chemicals and reagents

Cadmium acetate dehydrate, zinc acetate dehydrate, cuprous chloride and thiourea were obtained from Sinopharm Chem. Re. Co., Ltd. (Shanghai, China). PSA standards were the products of Abcam (Hong Kong, China). Monoclonal anti-PSA capture antibody (mAb) was acquired from BiosPacific, Inc. (CA, USA). Carboxylated magnetic bead (MB) was purchased from Aladdin (Shanghai, China). 1-Ethyl-3-(3-dimethylaminopropyl) carbodiimide hydrochloride (EDC) and N-hydroxysuccinimide (NHS) were obtained from Sigma-Aldrich (St. Louis, MO, USA). T4 DNA ligase, Phi29 DNA polymerase and exonuclease III (Exo III) were purchased from Thermo Fisher Scientific Inc. (Shanghai, China). dNTPs were purchased from Sangon Biotech. Co., Ltd. (Shanghai,

China). All other chemicals used in this work were of analytical grade. Water was purified with Millipore water purification system (18.25 MΩ cm^{-1}, Milli-Q, Millipore) and used throughout the work. All oligonucleotides were synthesized by Dingguo Biotechnol. Co., Ltd. (Beijing, China), and the sequences are listed below:

PSA aptamer-primer probe (apt-pri):

5'-ATTAAAGCTCGCCATCAAATAGCTTATTA*TGTCCGTGCTA***GAAGGAAACAGTTAC**-3'.

Linear padlock DNA:

5'-phosphate-*TAGCACGGACA*CGTATCGTATGTTCGCGTATCGTATGTTCG**GTAACTGTTTCCTTC**-3'.

G-rich DNA: 5'-TTGGGTAGGGCGGGTTGGGCGTATCGTATGTTCG-3'.

(note: in the PSA apt-pri, the underlined sequence was the aptamer of PSA, and the italic/bold sequences were complementary with those of linear padlock DNA, respectively.)

2.2. Fabrication of p-type Cu-doped $Zn_{0.3}Cd_{0.7}S$

The p-type Cu-doped $Zn_{0.3}Cd_{0.7}S$ photosensitive materials were synthesized by a hydrothermal treatment according to the literature with minor modification (Wu et al., 2016a). $Cd(Ac)_2{\cdot}2H_2O$ (2.5 mmol) and $Zn(Ac)_2{\cdot}2H_2O$ (1.07 mmol) were initially dissolved into 40-mL distilled water containing triethanolamine (5.0 mL, 3.5 M) and ammonia solution (5.0 mL, 14.4 M) under vigorous stirring. Subsequently, CuCl (21 mg) was dispersed into the above solution. Following that, the thiourea solution (5.0 mL, 1.0 M) was added dropwise into the above mixture slowly under magnetic stirring. After that, the resulting mixture was transferred into Teflon-lined stainless steel autoclave and kept at 180 °C for 10 h. The obtained products were washed with distilled water and ethanol alternately, and finally dried in a vacuum oven at 60 °C. The yield of Cu-doped $Zn_{0.3}Cd_{0.7}S$ was ~53.9%.

2.3. Conjugation of magnetic beads with monoclonal capture antibody (MB-mAb)

In the work, the monoclonal capture antibody was immobilized on the surface of carboxylated magnetic beads by a typical carbodiimide coupling (Lin et al., 2017; Qin et al., 2012). Before conjugation with mAb, the beads (1.0 mL, 5.0 mg mL^{-1}) were washed with MES buffer for three times, and then dispersed in the 1.0 mL of MES solution (pH 6.0) containing 0.1 M NHS and 0.4 M EDC. The resulting mixture was incubated on a shaker for 30 min at ambient temperature to

activate the −COOH groups on MB. After that, the functional magnetic beads were washed several times with buffer and then resuspended in an aqueous solution of monoclonal capture antibody (1.0 mL, 400 μg mL^{-1}). Following that, the mixture was shaken on a shaker overnight at 4 °C. The excess antibody was separated by using a magnet. Afterward, the MB-mAb conjugates were added into 1.0 mL of PBS (pH 7.4) containing 2.0 % BSA and incubated at 37 °C for another 2 h, and washed with PBS (pH 7.4). Finally, the as-prepared MB-mAb conjugates were dispersed in 1.0 mL of PBS (containing 1.0 wt % BSA and 0.02 % sodium azide, pH 7.4) and stored at 4 °C.

2.4. Capture antibody-target-aptamer reaction on MB with RCA

50 μL of as-prepared MB-mAb conjugates (5.0 mg mL^{-1}) and 50 μL of PSA standard/sample were injected into a centrifugal tube, and then incubated for 1 h at 37 °C under slight shaking. Then, the resulting mixture was magnetically separated and washed with PBS buffer (pH 7.4) for several times. Following that, 50 μL of PSA aptamer-primer probe (1.0 μM) was added into the tube and incubated for 40 min at 37 °C, then the magnetic mixture was collected and washed as before. Next, the resultant precipitate was incubated with 50-μL ligation reaction solution containing 1×T4 DNA ligase buffer (40 mM Tris-HCl, 10 mM $MgCl_2$, 10 mM dithiothreitol, 0.5 mM ATP, pH 7.8), padlock DNA (10 μL, 1.0 μM), and T4 DNA ligase (20 U) at 37 °C for 2 h. After magnetic separation and washing as before, the RCA reaction (induced by the primer-circular DNA on MB) was conducted in a 50-μL reaction buffer [Tris-HAc buffer (33 mM, pH 7.9) containing 10 mM $Mg(Ac)_2$, 66 mM KAc, 0.1% (v/v) Tween 20, 1.0 mM DTT, 1.0 mM dNTPs, and 5 U Phi29 DNA polymerase]. The reaction mixture was carried out for 50 min at 37 °C, and terminated by removing the reaction solution. Following that, the resulting product was blended with 50 μL of solution that contained hemin (5.0 μM), KCl (20 mM), and G-rich DNA (10 μM), and incubated for 80 min at 37 °C. Afterward, the magnetic product with hemin/G-quadruplex was collected and washed to remove the excess hemin and G-rich DNA. After that, the collected magnetic complex was re-dispread in 50 μL of Exo III (40 U) and incubated for 70 min at 37 °C. Finally, the reaction product after magnetic separation was transferred to the detection cell for the subsequent photocurrent measurement.

2.5 Photocurrent measurement

Prior to measurement, the fluorine-doped tin oxide (FTO) glass electrode was ultrasonically cleaned in water, acetone, ethanol, and water in sequence, and then was dried at 60 °C. Next, 25 μL of Cu-doped $Zn_{0.3}Cd_{0.7}S$ suspension (5.0 mg mL^{-1}, dispersed in water) (note: Prior to use, the sample was sonicated for several minutes to obtain a homogeneous suspension, and this suspension was stable within 30 min) was dropped onto the FTO glass with a fixed area of 0.28 cm^2. After being dried, the Cu-doped $Zn_{0.3}Cd_{0.7}S$-modified FTO glass was used as the working electrode, and the photocurrent measurement was carried out by using a conventional three-electrode system containing a Pt-wire counter electrode and an Ag/AgCl reference electrode with an applied potential of -400 mV. The photocurrent was recorded in 0.1 M Na_2SO_4 (N_2 was bubbled to remove dissolved oxygen before use) under the irradiation of 500 W Xe lamp (NBET, Beijing, China) on an AutoLab electrochemical workstation (μAutIII.Fra2.v, Eco Chemie, Netherlands).

3. Results and discussion

3.1. Characterization of Cu-doped $Zn_{0.3}Cd_{0.7}S$

The surface structure and morphology of the as-synthesized Cu-doped $Zn_{0.3}Cd_{0.7}S$ were first investigated by scanning electron microscopy (SEM). As seen in Fig. 1A, the Cu-doped $Zn_{0.3}Cd_{0.7}S$ sample exhibited a sphere-like shape with an average size of 1-3 μm in diamter. The magnified image displayed that the solid sphere was an agglomeration of small particles (inset of Fig. 1A). We also used energy dispersive spectroscopy (EDS) to confirm the element composition of the semiconductor. As shown in Fig. 1B, four elements including Cu, Zn, Cd, and S appeared in the sample. Moreover, powder X-ray diffraction (XRD) was used to investigate the crystalline structure of the as-prepared samples. As seen from curve 'a' in Fig. 1C, the main strong diffraction peaks in $Zn_{0.3}Cd_{0.7}S$ solid solutions were accordance with the previous reports (Wu et al., 2016a; Li et al., 2010), indicating that the successful synthesis of $Zn_{0.3}Cd_{0.7}S$. Upon doping of Cu^+ ions, the obtained XRD patterns were almost identical to that of $Zn_{0.3}Cd_{0.7}S$ alone (Fig. 1C, curve 'b'), and no traces of diffraction peaks corresponding to Cu were observed, which may be due to the small amount of Cu in the composite. In addition, we also utilized UV-visible diffuse reflectance spectrum (DRS) to study the optical absorption performance and corresponding bandgap energy (Eg) values of $Zn_{0.3}Cd_{0.7}S$ solid solutions before and after doping with cuprous ions. As seen from Fig. 1D, both

composites had significant absorption bands in the range of visible light, and the doping of Cu^{+} could enhance the light absorption capability of solid solutions in the visible light region (curve 'b' *vs.* curve 'a'), which was beneficial to improve the photocurrent response. The bandgab energies of composites shown in Fig. 1E were estimated from the DRS data [note: The corresponding calculation was based on the equation 1: $(\alpha h\nu)^2 = C\ (h\nu\text{-}Eg)$, where α, hν, C and Eg are the absorption coefficient, photo energy, the constant, and band gap energy, respectively (Long et al., 2015)]. Fig. 1F displayed the Mott-Schottky plots of Cu-doped $Zn_{0.3}Cd_{0.7}S$, the negative slope showed that the sample was p-type semiconductor, which further validated the successful synthesis of the photoactive material (Li et al., 2018).

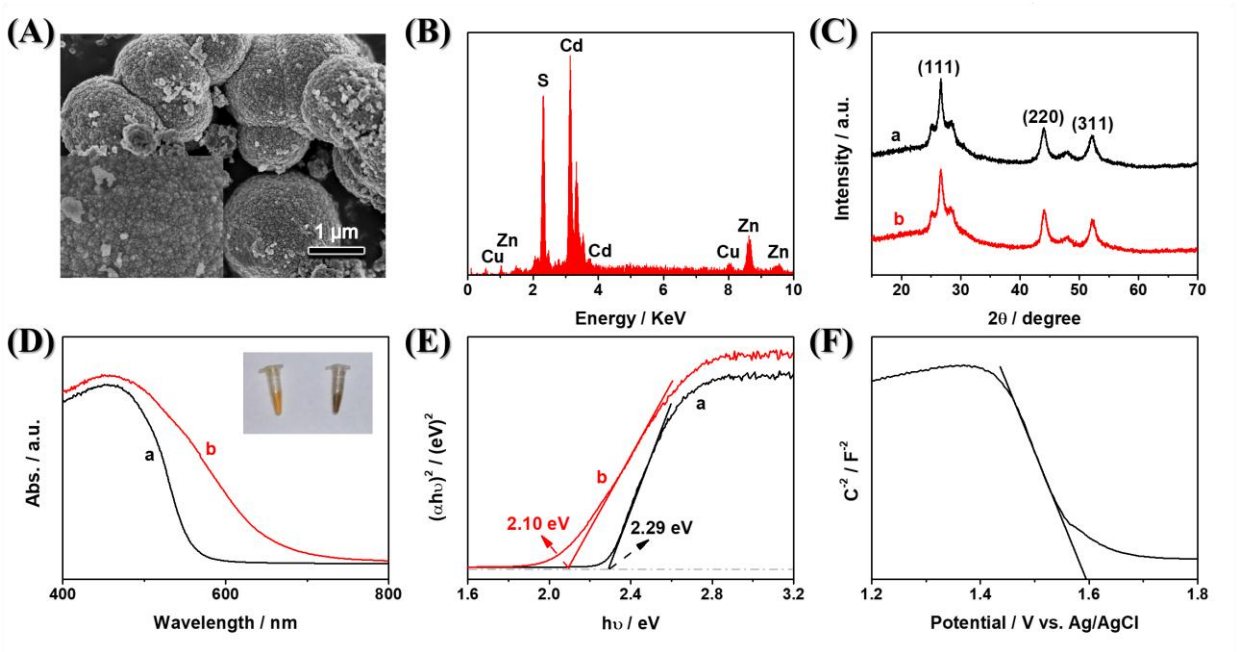

Fig. 1. (A) SEM image (inset: high-resolution image) and (B) EDS pattern of Cu-doped $Zn_{0.3}Cd_{0.7}S$; (C) XRD pattern, (D) UV-vis DRS spectrum [inset: photograph of (left) $Zn_{0.3}Cd_{0.7}S$ and (right) Cu-doped $Zn_{0.3}Cd_{0.7}S$] and (E) plots of $(\alpha h\nu)^2$ *vs.* photon energy (hν) of (a) $Zn_{0.3}Cd_{0.7}S$ and (b) Cu-doped $Zn_{0.3}Cd_{0.7}S$; (F) Mott-Schottky plots of Cu-doped $Zn_{0.3}Cd_{0.7}S$.

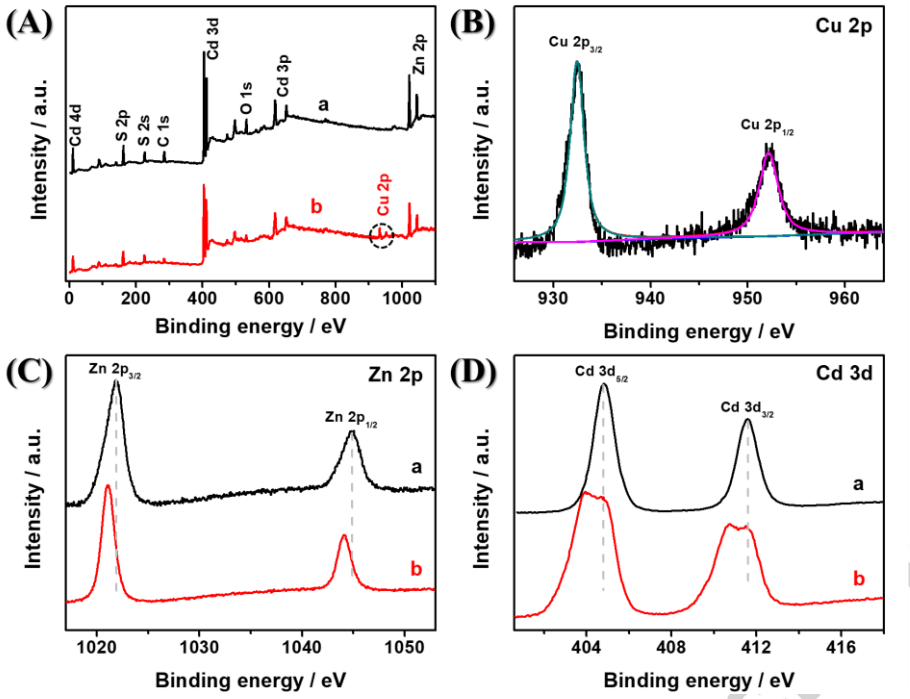

Fig. 2. (A) The overall XPS spectra of (a) $Zn_{0.3}Cd_{0.7}S$ and (b) Cu-doped $Zn_{0.3}Cd_{0.7}S$; (B) high-resolution XPS spectrum of Cu in Cu-doped $Zn_{0.3}Cd_{0.7}S$; high-resolution XPS spectra of (C) Zn and (D) Cd in (a) $Zn_{0.3}Cd_{0.7}S$ and (b) Cu-doped $Zn_{0.3}Cd_{0.7}S$.

X-ray photoelectron spectroscopy (XPS) technology was further employed to characterize the surface composition and chemical state of various elements in the prepared semiconductor samples. Fig. 2A depicted the full survey spectra of undoped and doped $Zn_{0.3}Cd_{0.7}S$. As expected, Zn, Cd, and S elements were present in both scan spectra (curve 'a' and 'b'), and Cu element only existed in the curve 'b'. From the high-resolution XPS spectrum of Cu 2p in Cu-doped $Zn_{0.3}Cd_{0.7}S$ (Fig. 2B), the binding energy values at 932.5 eV and 952.4 eV corresponded to Cu $2p_{3/2}$ and Cu $2p_{1/2}$, respectively. These binding energies agreed well with that of Cu^{+} (Wu et al., 2016b), indicating that the Cu element may exist in the form of Cu^{+}. XPS spectrum of Zn 2p in undoped $Zn_{0.3}Cd_{0.7}S$ (Fig. 2C, curve 'a') displayed two peaks located at 1021.9 eV (Zn $2p_{3/2}$) and 1044.9 eV (Zn $2p_{1/2}$), suggesting that the valence state of Zn element is +2 (Li et al., 2013). As shown in Fig. 2D, two fitted peaks from Cd 3d in $Zn_{0.3}Cd_{0.7}S$ (curve 'a') at 404.9 eV and 411.6 eV could be attributed to Cd $3d_{5/2}$ and Cd $3d_{3/2}$, respectively, which were in line with the previous report (Guo et al., 2015). It is worth noting that the doping of Cu element could significantly shift the binding energy values of Zn 2p (curve 'b' in Fig. 2C) and Cd 3d (curve 'b' in Fig. 2D), which might be related to the

chemical interaction between Zn, Cd, and Cu in the doped solid solutions.

3.2. Feasibility evaluation of the designed PEC sensing platform

Scheme 1 illustrates the detailed principle of the designed sensing platform. In this system, the monoclonal capture antibody coated magnetic bead (MB-mAb) and aptamer-primer probe could specifically recognize target PSA, and the sandwiched complex of MB-mAb/PSA/apt-pri would be formed after the introduction of PSA. With the help of ligase and polymerase, the aptamer-primer probe could hybridize with linear padlock DNA (as the circular template) and initiate the RCA reaction. Two repeated segments containing 15 bases in the middle of the circular template were designed to be identical to 15 bases at the 3' end of the G-rich DNA. As a result, the resulting RCA product contains thousands of repeated sequences, and each repeated sequence in the RCA product could hybridize with G-rich DNA to form a DNA duplex with a blunt 3'-termini. Then, the remaining bases of G-rich DNA could bind with hemin to form hemin/G-quadruplex. Upon the addition of Exo III, the formed duplex DNA probe could be digested, thereby releasing numerous liberated hemin/G-quadruplex (used as electron acceptors) and leading to the increasing photocurrent of the Cu-doped $Zn_{0.3}Cd_{0.7}S$-modified FTO electrode. On the contrast, the RCA reaction and the subsequent process would not proceed in the absence of PSA, thus, no significant photocurrent change could be observed. Hence, we can evaluate the concentration of target PSA in the test sample by monitoring the change in the photocurrent.

The photocurrent generation mechanism on the Cu-doped $Zn_{0.3}Cd_{0.7}S$ is illustrated in Fig. S1 (Supporting Information). Electrons/holes are generated when the photoactive material is irradiated with light. The photogenerated electrons on the conduction band of Cu-doped $Zn_{0.3}Cd_{0.7}S$ would be captured by the electron acceptors in solution, and the photogenerated holes on the valence band would be neutralized by the electrons from FTO electrode, generating a cathodic photocurrent. To confirm that hemin could increase the photocurrent of Cu-doped $Zn_{0.3}Cd_{0.7}S$-modified FTO via a PET mechanism, DRS and Mott-Schottky plots were used to study the conduction band and valence band edges of Cu-doped $Zn_{0.3}Cd_{0.7}S$. The flat band potential of p-type semiconductor is considered to be approximately equal to its valence band (Li et al., 2018). Thus, the valence band edge of Cu-doped $Zn_{0.3}Cd_{0.7}S$ was located at around 1.59 V *vs* Ag/AgCl (Fig. 1F). Combined with the band gap obtained from DRS data, the conduction band edge of Cu-doped $Zn_{0.3}Cd_{0.7}S$ was estimated to

be -0.51 V vs Ag/AgCl (-0.31 V vs normal hydrogen electrode (NHE)). The hemin in hemin/G-quadruplex complex displayed a reduction potential of -0.026 V vs NHE (Sharon et al., 2010). On the basis of the above results, the redox state of hemin/G-quadruplex complex and the band positions of Cu-doped $Zn_{0.3}Cd_{0.7}S$ relative to the potentials of NHE were displayed in Scheme 1B. It could be found that the conduction band level of this semiconductor was more negative than the reduction potential of hemin/G-quadruplex, implying that the photoexcited electrons on the conduction band of Cu-doped $Zn_{0.3}Cd_{0.7}S$ could be transferred to the hemin.

As mentioned above, the RCA product provides the binding sites for hemin/G-quadruplex and acts a pivotal part in the signal amplification. To verify the RCA reaction, agarose gel electrophoresis was employed (Fig. 3A). As seen from lane 'a', the bright spots were observed at the initial position of the lane, suggesting the low mobility of the RCA product. Obviously, the number of bases in the RCA product was far beyond 1500 bp, revealing that the RCA reaction was successfully carried out. In contrast, no spot was observed in the control experiment (lane 'b'), indicating that the RCA reaction could not occur in the absence of primer. Next, several control experiments were used to further verify the feasibility of Cu-doped $Zn_{0.3}Cd_{0.7}S$-based PEC sensing system for the detection of PSA (Fig. 3B). The table showed the substance that was missing during the entire reaction. Curve 'a' displayed the background photocurrent of Cu-doped $Zn_{0.3}Cd_{0.7}S$-modified FTO. As shown in curve 'b', almost no photocurrent change was observed, indicating that the sandwiched complex (MB-mAb/PSA/apt-pri) could not be formed in the absence of target PSA. This result was consistent with the result of gel electrophoresis. In our design, hemin, which act as an electron acceptor, could capture photogenerated electrons from Cu-doped $Zn_{0.3}Cd_{0.7}S$-modified electrode to significantly enhance its photocurrent response. Without the addition of hemin solution, no obvious enhancement of the photocurrent was observed (curve 'c'). In addition, the absence of Exo III could not cause significant photocurrent change (curve 'd'), the reason was attributed to the fact that hemin/G-quadruplex was trapped on the RCA product and could not be released into the solution. As depicted in curve 'e', the photocurrent largely increased when the target PSA, hemin and Exo III were added in the order of the experimental procedures. All of the above results demonstrated that the developed PEC sensing platform for the detection of PSA was feasible.

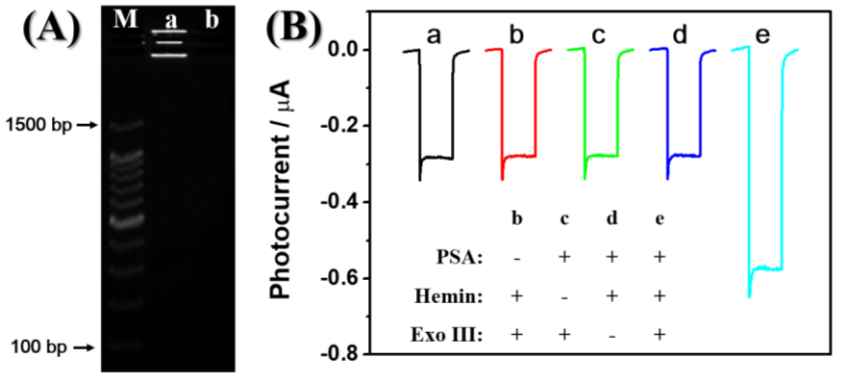

Fig. 3. (A) Agarose gel electrophoresis (M: DNA marker; lane a: RCA product; lane b: control experiment, without aptamer-primer probe); (B) photocurrents of Cu-doped $Zn_{0.3}Cd_{0.7}S$-modified FTO electrode in different components (+: with, −: without) (note: curve '*a*' presents the photocurrent of newly prepared Cu-doped $Zn_{0.3}Cd_{0.7}S$-modified FTO) (1.0 ng mL^{-1} target PSA used in this case).

3.3. Optimization of experimental conditions

To maximize the analytical performance of the developed sensing method, the effects of several experimental parameters including PSA-aptamer reaction time, RCA reaction time, and digestion time of Exo III on the performance of this sensing platform were investigated. The incubation time for PSA-aptamer reaction played a crucial role in achieving an excellent performance of our sensing method. In fact, the procedure was important because it affected the subsequent signal amplification steps in our design and indirectly affected the amount of free hemin/G-quadruplex in the detection cell. As exhibited in Fig. S2A, along with increasing the incubation time, we observed a gradually increasing photocurrent in the 5-40 min time range, and the photocurrent response remained stable after 40 min. Thus, 40 min was chosen as the incubation time for PSA-aptamer reaction. Obviously, it takes some time for the polymerase to generate the RCA long product for capturing hemin/G-quadruplex, and a short reaction time is not conducive to the formation of the long strand. As shown in Fig. S2B, with the extension of RCA reaction time, a continuous increased photocurrent was observed in the range of 10-50 min, while the photocurrent reached a plateau after 50 min. A longer reaction time did not markedly enhance the photocurrent. Therefore, 50 min was selected as the optimal reaction time for RCA. The hemin/G-quadruplex released by the digestion of Exo III could heavily affect the signal of the sensing platform, and the digestion time directly influenced the amount of liberated hemin/G-quadruplex. As depicted in Fig. S2C, the photocurrent

increased with the time aged, and then tended to level off when the digestion time exceeded 70 min. To save the assay time, 70 min was employed as the digestion time for Exo III.

3.4. Analytical performance of Cu-doped $Zn_{0.3}Cd_{0.7}S$-based PEC sensing platform

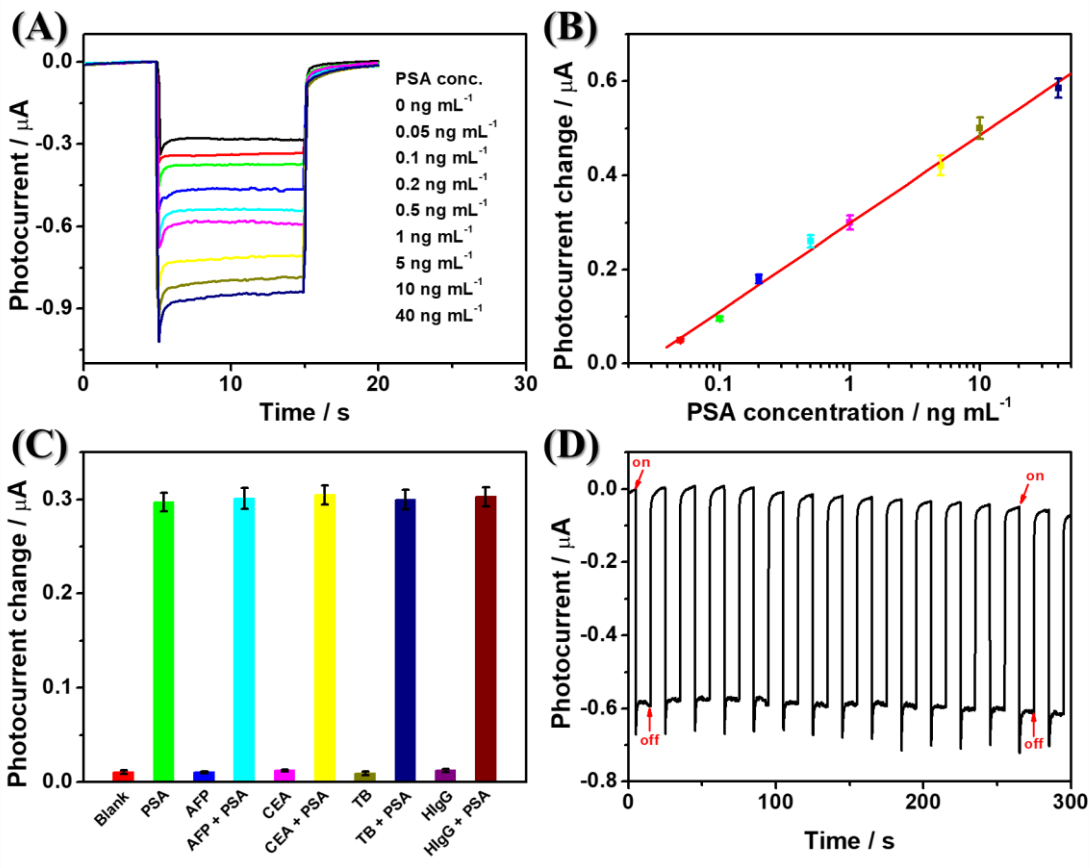

Fig. 4. (A) Photocurrent responses of Cu-doped $Zn_{0.3}Cd_{0.7}S$-based sensing platform toward target PSA with different concentrations; (B) the corresponding calibration plots; (C) the specificity of the proposed PEC sensing method against target PSA (1.0 ng mL^{-1}), AFP (40 ng mL^{-1}), CEA (40 ng mL^{-1}), thrombin (40 ng mL^{-1}), and human IgG (40 ng mL^{-1}); (D) The stability of Cu-doped $Zn_{0.3}Cd_{0.7}S$-based sensing platform under the repeated 'on↔off' light irradiation (1.0 ng mL^{-1} target PSA used in this case).

On the basis of the optimized conditions, the analytical performance of the proposed Cu-doped $Zn_{0.3}Cd_{0.7}S$-based PEC sensing platform was evaluated by assaying different concentrations of PSA standards. As exhibited in Fig. 4A, the photocathodic current of the PEC sensor was observed to increase stepwise with increasing PSA concentration in the samples. The calibration curve of the shift in the photocathodic current versus the logarithm value of PSA concentration ranging from 0.05 ng mL^{-1} to 40 ng mL^{-1} displayed a good linearity (Fig. 4B). The linear regression equation was

ΔI (μA) = 0.1874 × lg($C_{[PSA]}$/ng mL^{-1}) + 0.2985 (R^2 = 0.9948, n = 8). And the detection limit (LOD) was calculated to be 16.3 pg mL^{-1}. Compared with several previously reported strategies for the detection of PSA (Table S1 in the Supporting information), the linear range and detection limit of the developed PEC sensor were quite satisfactory.

Furthermore, several common biomolecules, such as alpha-fetoprotein (AFP), carcinoembryonic antigen (CEA), thrombin (TB), and human IgG (HIgG) were introduced as the interference proteins to evaluate the selectivity and specificity of the PEC detection system. The evaluation was carried out by comparing with the change in the photocurrent relative to the background signal. Initially, these non-targets were measured separately, and then their mixture including 1.0 ng mL^{-1} PSA and 40 ng mL^{-1} non-target were determined by using the same detection mode. As seen from Fig. 4C, the photocurrents of our system toward non-targets including AFP, CEA, TB and HIgG alone were almost the same as background signal, and a strong photocurrent was acquired for target PSA. Favorably, coexistence of non-targets with target PSA did not cause significant change in the photocurrent. These results revealed that the Cu-doped $Zn_{0.3}Cd_{0.7}S$-based PEC sensing platform had a good selectivity and high anti-interference ability. As a key parameter in the application of sensor, the stability of the proposed PEC sensing platform was investigated by recording the photocurrent response under the repeated irradiation. As depicted in Fig. 4D, no significant fluctuations in cathodic photocurrent were observed, demonstrating a good stability. Also, we evaluated the reproducibility of this method by analyzing five parallel measurements on the basis of different-batch photosensitive electrodes toward five same-concentration PSA standards (1.0 ng mL^{-1} PSA used as an example), respectively, and the relative standard deviation (RSD) was 7.6%, suggesting a satisfactory acceptable reproducibility.

3.5. Application of the proposed PEC sensing system in human serum samples

To evaluate the accuracy and reliability of the newly proposed PEC sensing method in real samples, several human serum samples, which were collected from the local hospital, were analyzed by using commercialized PSA ELISA kit and the developed method, respectively. The values of t_{exp} between the referenced ELISA method and the developed PEC method were calculated by using a t-test statistical analysis, and the experimental results are summarized in Table 1. All t_{exp} values in these tests were below the t_{crit} ($t_{crit[0.05,4]}$ = 2.77), no significant differences were

found at the confidence level of 95%, displaying a good accuracy between the two methods. Thus, the proposed Cu-doped $Zn_{0.3}Cd_{0.7}S$-based PEC sensing platform exhibited its potential in clinical diagnosis and could be utilized as a reliable method for PSA determination in the complex biological system.

Table 1 Comparison of the assay results by using the proposed PEC sensing platform and the ELISA method

Sample no.	Method; Concentration (mean ± SD, ng mL^{-1}, n = 3)		t_{exp}
	PEC sensing method	PSA ELISA kit	
1	0.74 ± 0.06	0.81 ± 0.07	1.32
2	1.87 ± 0.14	1.98 ± 0.16	0.90
3	0.19 ± 0.02	0.22 ± 0.02	1.84
4	14.52 ± 1.12	15.01 ± 1.25	0.51
5	7.17 ± 0.46	6.85 ± 0.61	0.73
6	24.93 ± 1.78	26.34 ± 1.57	1.03

Conclusions

In summary, a novel photoelectrochemical sensing platform for the sensitive detection of PSA based on p-type Cu-doped $Zn_{0.3}Cd_{0.7}S$ solid solutions and target-triggered rolling circle amplification was successfully fabricated. Experimental results revealed that the PEC biosensors exhibited high sensitivity, good reproducibility/specificity, and acceptable accuracy in comparison with commercial ELISA kits. The photocathodic current originated from the Cu-doped $Zn_{0.3}Cd_{0.7}S$ semiconductor and was enhanced by the hemin/G-quadruplex complexes in the solution. Compared with the commonly used n-type semiconductors, introduction of p-type Cu-doped $Zn_{0.3}Cd_{0.7}S$ could avoid the interference of some coexisting reducing substances. Meanwhile, the design of the split-type assay mode could avoid the damage of biomolecules in the measurement process and effectively improve the stability and performance of the PEC sensing method. Nevertheless, one limitation of our strategy is that the entire assay process was cumbersome, resulting in a relatively long assay time. Thus, future work should focus on the improvement of the detection process.

Although the present method was applied for the detection of target PSA, importantly, it easily extends to determine other cancer biomarkers by controlling the corresponding antibody and aptamer.

Acknowledgments

This work was financially supported by the National Natural Science Foundation of China (21675029 & 21475025), the National Science Foundation of Fujian Province (2014J07001), and the Program for Changjiang Scholars and Innovative Research Team in University (IRT15R11).

References

Alizadeh, N., Hallaj, R., Salimi, A., 2017. Biosens. Bioelectron. 94, 184-192.

Chen, X., Xu, W., Jiang, Y., Pan, G., Zhou, D., Zhu, J., Wang, H., Chen, C., Li, D., Song, H., 2017. Nanoscale 9, 16357-16364.

Chinen, A., Guan, C., Ferrer, J., Barnaby, S., Merkel, T., Mirkin, C., 2015. Chem. Rev. 115, 10530-10574.

Cong, X., Fan, G., Wang, X., Abdel-Halim, E., Zhu, J., 2016. J. Mater. Chem. B 4, 6117-6124.

Dai, W., Zhang, L., Zhao, W., Yu, X., Xu, J., Chen, H., 2017. Anal. Chem. 89, 8070-8078.

Deng, M., Zhang, D., Zhou, Y., Zhou, X., 2008. J. Am. Chem. Soc. 130, 13095-13102.

Eivazzadeh-Keihan, R., Pashazadeh-Panahi, P., Baradaran, B., Maleki, A., Hejazi, M., Mokhtarzadeh, A., de la Guardia, M., 2018. Trends Anal. Chem. 100, 103-115.

Fan, D., Ren, X., Wang, H., Wu, D., Zhao, D., Chen, Y., Wei, Q., Du, B., 2017. Biosens. Bioelectron. 87, 593-599.

Gao, Y., Li, B., 2013. Anal. Chem. 85, 11494-11500.

Guo, S., Min, Y., Fan, J., Xu, Q., 2015. ACS Appl. Mater. Interfaces 8, 2928-2934.

Kaur, M., Nagaraja, C., 2017. ACS Sustain. Chem. Eng. 5, 4293-4303.

Kulasingam, V., Diamandis, E., 2008. Nat. Clin. Pract. Oncol. 5, 588–599.

Li, W., Li, D., Chen, Z., Huang, H., Sun, M., He, Y., Fu, X., 2008. J. Phys. Chem. C. 112, 14943-14947.

Li, W., Li, D., Zhang, W., Hu, Y., He, Y., Fu, X., 2010. J. Phys. Chem. C. 114, 2154-2159.

Li, W., Li, D., Meng, S., Chen, W., Fu, X., Shao, Y., 2011. Environ. Sci. Technol. 45, 2987-2993.

Li, F., Chen, G., Luo, J., Huang, Q., Luo, Y., Meng, Q., Li, D., 2013. Catal. Sci. Technol. 3, 1993-1999.

Li, Z., Xin, Y., Zhang, Z., 2015. Anal. Chem. 87, 10491-10497.

Li, J., Griep, M., Choi, Y., Chu, D., 2018. Chem. Commun. 54, 3331-3334.

Lin, Y., Zhou, Q., Tang, D., Niessner, R., Knopp, D., 2017. Anal. Chem. 89, 5637-5645.

Liu, Y., Xiong, E., Li, X., Li, J., Zhang, X., hen, J., 2017. Biosens. Bioelectron. 87, 970-975.

Long, B., Huang, Y., Li, H., Zhao, F., Rui, Z., Liu, Z., Tong, Y., Ji, H., 2015. Ind. Eng. Chem. Res. 54, 12788-12794.

Lv, S., Zhang, K., Lin, Z., Tang, D., 2017. Biosens. Bioelectron. 96, 317-323.

Pang, X., Pan, J., Wang, L., Ren, W., Gao, P., Wei, Q., Du, B., 2015. Biosens. Bioelectron. 71, 88-97.

Qin, G., Zhao, S., Huang, Y., Jiang, J., Ye, F., 2012. Anal. Chem. 84, 2708-2712.

Ren, W., Zhang, Y., Huang, W., Li, N., Luo, H., 2015. Biosens. Bioelectron. 68, 266-271.

Sharon, E., Freeman, R., Willner, I., 2010. Anal. Chem. 82, 7073-7077.

Shu, J., Qiu, Z., Lin, Z., Cai, G., Yang, H., Tang, D., 2016. Anal. Chem. 88, 12539-12546.

Tang, J., Kong, B., Wang, Y., Xu, M., Wang, Y., Wu, H., Zheng, G., 2013. Nano Lett. 13, 5350-5354.

Tang, G., Zhao, C., Gao, J., Tan, H., 2016. Sens. Actuators, B. 237, 795-801.

Wang, W., Bao, L., Lei, J., Tu, W., Ju, H., 2012. Anal. Chim. Acta 744, 33-38.

Wang, G., Shu, J., Dong, Y., Wu, X., Zhao, W., Xu, J., Chen, H., 2015. Anal. Chem. 87, 2892-2900.

Wu, Y., Yue, Z., Liu, A., Yang, P., Zhu, M., 2016a. ACS Sustain. Chem. Eng. 4, 2569-2577.

Wu, W., Chakrabortty, S., Guchhait, A., Wong, G., Dalapati, G., Lin, M., Chan, Y., 2016b. Chem. Mater. 28, 9132-9138.

Xu, X., Lu, R., Zhao, X., Zhu, Y., Xu, S., Zhang, F., 2012. Appl. Catal. B-Environ. 125, 11-20.

Zhao, W., Ma, Z., Xu, J., Chen, H., 2013. Anal. Chem. 85, 8503-8506.

Zhang, K., Lv, S., Lin, Z., Li, M., Tang, D., 2018. Biosens. Bioelectron. 101, 159-166.

Zhou, W., Gong, X., Xiang, Y., Yuan, R., Chai, Y., 2013. Anal. Chem. 86, 953-958.

Zhou, Z., Yu, Y., Zhang, M., Chen, J., Ren, Q., Song, J., Liu, B., Ma, Z., Zhao, Y., 2014. Sens. Actuators, B. 201, 496-502.

Highlights:

- A photoelectrochemical biosensing platform was designed for PSA detection.
- The p-type Cu-doped $Zn_{0.3}Cd_{0.7}S$ was used as the photosensitive materials.
- Rolling circle amplification and exonuclease III were utilized for the signal amplification.
- Hemin/G-quadruplex complex was used as an electron acceptor for Cu-doped $Zn_{0.3}Cd_{0.7}S$.